Hairy self-assemblies of surfactants



2005 J. Phys.: Condens. Matter 17 S2911

(http://iopscience.iop.org/0953-8984/17/31/018)

INSTITUTE OF PHYSICS PUBLISHING JOURNAL OF PHYSICS: CONDENSED MATTER

J. Phys.: Condens. Matter **17** (2005) S2911–S2922 doi:10.1088/0953-8984/17/31/018

# Hairy self-assemblies of surfactants

**C Ligoure**

GDPC, UMR CNRS 5581, CC 26, Université Montpellier 2, 34095 Montpellier Cedex 05, France

E-mail: ligoure@gdpc.univ-montp2.fr

Received 20 December 2004, in final form 26 January 2005
Published 22 July 2005
Online at stacks.iop.org/JPhysCM/17/S2911

**Abstract**

Surfactant-containing systems are characterized by the self-assembly of aggregated units that endow the bulk level with emergent physical properties. The aggregates themselves take on different shapes from lamellae to spheres. During the last decade the soft matter complexity in this field has been contributed by the polymeric component. I will focus on the addition of amphiphilic copolymers in structured surfactant phases on simple shapes, i.e., flat bilayers, cylinders and spheres. In all cases, the hydrophobic block of the copolymer adsorbs on the surfactant layer, whereas the hydrophilic tails remain in the aqueous solvent and decorate the film. The guest component modifies both the elastic properties of the film and the interactions between the surfactant mesoscopic objects. Small angle neutron scattering is the main experimental technique we used to reveal and analyse some of these polymer-induced modifications.

(Some figures in this article are in colour only in the electronic version)

## 1. Introduction

Surfactants or lipids in solution usually form supra-molecular assemblies of various shapes, such as spherical micelles or micro-emulsions, cylindrical giant micelles and periodically stacked sheets of bilayers (lamellar phases). Complex systems consisting of self-assemblies of surfactants and guest components such as polymers or colloidal particles are widely recognized in the fields of biological membranes, drug carrier systems, lubricants, cosmetics, etc. Interactions between the guest component and the host phase can induce strong modifications of the physical properties of the host phase. Indeed, the guest component can change both the elastic moduli of the amphiphilic film and the interactions between the aggregates, and finally the rheological properties of the solution. In this paper, I will focus on 'hairy surfactant self-assemblies' with simple shapes. 'Hairy' aggregates are obtained by adding to solutions of surfactants a small amount of amphiphilic copolymer whose hydrophobic blocks anchor on the fluid surfactant films of the aggregates, and whose hydrophilic tails remain swollen

  

in the aqueous solvent and decorate them. Interestingly, for the experimental systems we have investigated, the morphologies of the initial host phases are preserved by addition of quite large amounts of added copolymer. This allows us to investigate the role of the block copolymer on the structure by quantitative analysis of small angle neutron scattering (SANS) data. Among the numerous effects of grafted polymer layers, I will highlight (i) the role of the anchored polymers to the *bending* properties of surfactant monolayers (section 2) and (ii) the peculiarities of the steric interaction induced by grafted polymer layers between *soft* interfaces (in contrast with the more classical steric repulsion between solid colloids) in sections 3 and 4. To address these questions, three simple geometries have been investigated: hairy oil-in-water microemulsion droplets in section 2, lamellar phase of hairy bilayers in section 3 and hairy cylinders consisting of wormlike micelles in section 4.

## 2. Hairy oil-in-water microemulsion droplets

The detailed report of this section can be found in [1]. The starting situation is a microemulsion of oil droplets in water stabilized by a monolayer of surfactant molecules. The evolution of the elastic properties of a surfactant film upon its decoration with a polymer anchored to the monolayer can be derived from the measurement of the mean radius and the polydispersity of the droplets [2, 3] by means of small angle neutron scattering [4]. For a droplet microemulsion the relevant bending parameters are $\tilde{\kappa} = \frac{1}{2}(2\kappa + \bar{\kappa})$ and $\tilde{C}_0 = \kappa C_0/\tilde{\kappa}$ with $\kappa$ and $\bar{\kappa}$, respectively, the mean and Gaussian bending modulus, and $C_0$ the spontaneous curvature.

We use a mixture of cetylpyridiniumchloride (CPCl) as surfactant, octanol (as cosurfactant), deuterated decane and brine (0.2 M NaCl). The polymer PEO-C12 is hydrophobically modified poly(ethylene oxide) of molecular weight $M \sim 5200$ Da. The volume fraction of the droplets in the initial naked microemulsion is 3.2%. The microemulsion is prepared at the microemulsion failure boundary, then the droplets have a radius corresponding to the optimum curvature of the surfactant film and a narrow size distribution. The samples are characterized by the amount $\sigma$ of copolymer per surfactant layer area. The hairy droplets have been prepared in such a way that some surfactant molecules are replaced by the copolymer in order to keep a practically constant shell volume fraction. More details can be found in [1]. SANS measurements have been performed at LLB-Saclay, on the spectrometer PACE under shell contrast conditions. Analysis of the scattered intensity indicates that, up to a rather large amount of copolymer, the droplets of microemulsion remain spherical and can be modelled as concentric shells with sharp boundaries. In fact decoration of the film with the polymer lowers the emulsion failure limit. From the spectra measured for various samples (bare to highly decorated microemulsions), we obtain the variation of the mean radius $\bar{R}_m$, the shell thickness $\delta$ and the standard deviation of the radius $\Delta R$ with $\sigma$ as described in detail in [1].

According to the model proposed by Milner and Safran [2], the optimum curvature radius of the droplets $R$ and the polydispersity $p$ ($p^2 = (\overline{R^2} - \overline{R}^2)/\overline{R}^2$) are related to $\tilde{\kappa}$, $\tilde{C}_0$ and $\phi$, the volume fraction of droplets:

$$\bar{R}\tilde{C}_0 = 1 + \frac{kT}{8\pi\tilde{\kappa}}\frac{1}{\phi}[\phi \ln \phi + (1-\phi)\ln(1-\phi)] \tag{1}$$

$$p^2 = \frac{kT\phi}{16\pi\tilde{\kappa}\phi + 2kT[\phi \ln \phi + (1-\phi)\ln(1-\phi)]}. \tag{2}$$

From equations (1), (2), and the values of $\phi$ and $\sigma$ deduced from the spectra, we derive the values of $\tilde{R}_0 = \tilde{C}_0^{-1}$ and $\tilde{\kappa}$ applying the equations at the outer of the surface of the droplets $\bar{R} = R_m + \delta/2$. The results are plotted in figure 1 as a function of $\sigma$ (symbols) together with a model developed below (full lines).

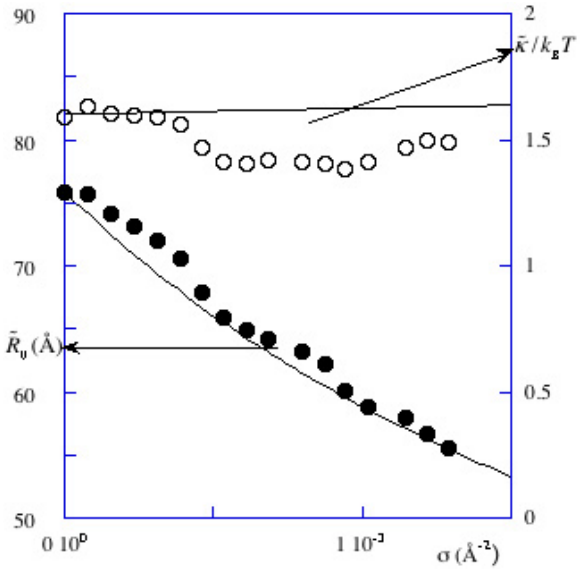


**Figure 1.** The elastic properties of a surfactant film as a function of its decoration with the anchoring of PEO-C12 measured by $\sigma$, the number of PEO-C12 per Å$^2$. The coefficient of rigidity $\tilde{\kappa}$ (open circles) is found to be almost constant (within experimental errors) and equal to $1.5 \pm 0.2kT$. The optimum radius of curvature (full dots) $\tilde{R}_0$ decreases slowly and monotonically. The calculated values are given by the lines (see the text for further discussion).

The theoretical model developed to predict the bending properties of flat fluid membranes decorated with small amounts of anchored polymers [5, 6] predicts a sharper decrease of the optimum radius of curvature than is observed in our experiments and a quite strong increase of the effective bending modulus $\tilde{\kappa}$ which is not observed in our experiments. We have identified two possible reasons for these discrepancies.

(i) The contribution of an ideal anchored polymer chain to the elastic curvature constants of a membrane has been calculated in the limit where the curvature radius of the film is much larger than the radius of gyration of the polymer chain [6]. This assumption becomes invalid when applied to strongly curved interfaces, as in our experiments where the radius of the droplets and the polymer coil size are of the same order of magnitude.

(ii) In fluid films, anchored polymers are free to diffuse on the surface of the monolayer and furthermore can exchange with the aqueous solvent reservoir. So $\sigma$ is not a locally conserved quantity and the mechanical properties of the mixed monolayer at fixed chemical potential $\mu$ (where $\mu$ is the potential conjugate to $\sigma$) are more relevant in this context [7].

A simple model can be built up, which contains both above-mentioned arguments. Let consider spherical droplets of radius $R = 1/C$ decorated with grafted ideal chains of polymerization index $N$. $R_G = a\sqrt{N}/\sqrt{6}$ is the radius of gyration, and $a$ is the monomer length. The free energy per unit area of the hairy microemulsion droplets in the mushroom regime (the mushroom regime extends up to the overlap coverage $\sigma^*$ at which point the anchored polymers on the droplet become to overlap) reads:

$$f_s = 2\tilde{\kappa}_{\text{bare}}(C - \tilde{C}_{0,\text{bare}})^2 - \sigma kT \ln\left(\frac{\alpha + aC}{1 + aC}\right) + kT\sigma \ln(\sigma a^2) \tag{3}$$

where $\tilde{\kappa}_{\text{bare}}$ and $\tilde{C}_{0,\text{bare}}$ are the elastic parameters of the bare droplet and $\alpha = \text{erf}(a/2R_g)$.

The first term in equation (3) is the bending energy of the bare film, the second term is the free energy of the anchored polymers (calculated using the Edward's propagator formalism) and the third one is the entropic contribution of the 2D gas of polymer anchors in the film. Notice that we have neglected steric interactions between mushrooms which would appear in equation (3) as a term proportional to $\sigma^2$. However, the prefactor (effective second order virial coefficient) is unknown and should not depend on the curvature in a first approximation; the contribution of the steric interactions should be weak ($\sigma < \sigma^*$) and should modify only slightly the effective spontaneous curvature and the effective bending modulus. However, as shown later, interpretations of the experimental results seem to be consistent without this contribution. The spontaneous curvature of the hairy microemulsion $\tilde{C}_{0,\sigma}$ at constant polymer area density $\sigma$ is then the single real solution of the cubic algebraic equation $\partial f_s/\partial C = 0$, whereas the bending modulus at constant $\sigma$ is given by $\tilde{\kappa}_\sigma = \frac{1}{4}\partial^2 f_s/\partial\sigma^2|_{C=\tilde{C}_{0,\sigma}}$. So we have properly taken into account item (i). However, equation (3) shows that the polymer composition of the membrane $\sigma$ couples to the curvature $C$; this coupling will play a significant role in the bending properties of the film, as the anchored polymers are free to diffuse in the membrane. Such properties can be interpreted in terms of spontaneous curvature $\tilde{C}_{0,\mu}$ and bending modulus $\tilde{\kappa}_\mu$ calculated at fixed chemical potential $\mu$ rather than at fixed composition $\sigma$ [7]. The chemical potential is the potential conjugate to $\sigma$:$\mu = \partial f_s/\partial\sigma$. We now calculate $\tilde{C}_{0,\mu}$ and $\tilde{\kappa}_\mu$ using the general theory built up in [7]:

$$\tilde{\kappa}_\mu = \tilde{\kappa}_\sigma - \left(\frac{\partial^2 f_s}{\partial C\,\partial\sigma}\right)^2 \Bigg/ \left.\frac{\partial^2 f_s}{\partial\sigma^2}\right|_{C=\tilde{C}_{0,\sigma}} \tag{4}$$

$$\tilde{C}_{0,\mu} = \frac{\tilde{\kappa}_\sigma}{\tilde{\kappa}_\mu}\tilde{C}_{0,\sigma}. \tag{5}$$

The theoretical values $R_{0,\mathrm{theo}} = \tilde{C}_{0,\mu}^{-1}$ and $\tilde{\kappa}_\mu$, given respectively by equations (4) and (5), are plotted in figure 1 (full lines) together with the experimental values. In these calculations, we set the polymerization index to $N = 113$ (the mean number of EO monomers in the chain), $\tilde{\kappa}_{\mathrm{bare}} = 1.6kT$ and $\tilde{C}_{0,\mathrm{bare}}^{-1} = 76$ Å are the experimental values measured for the bare microemulsion. The monomer length $a = 3.5$ Å is the only fitting parameter of the model (notice that choosing $a$ is a means of adapting the model to real chains, even though it is derived for Gaussian chains [8]). Both the decrease of $\tilde{R}_0$ and the constant value of $\tilde{\kappa}$ are correctly predicted by the model. This would not be the case if we chose for comparison with the experiments $\tilde{\kappa}_\sigma$ and $\tilde{C}_{0,\sigma}$ rather than $\tilde{\kappa}_\mu$ and $\tilde{C}_{0,\mu}$. These results clearly show that the free diffusion of polymers chains as well as their exchange with the reservoir plays a crucial role in the bending properties of spherical films. In particular, it leads to a quasi-invariance of the effective bending modulus upon variation of the chain coverage. This effect has already been observed for hairy vesicles [9].

## 3. Lamellar lyotropic phases of hairy bilayers

The detailed reports of this section can be found in [10–12]. Lamellar phases decorated with copolymers can be prepared: bilayers of thickness $\delta_0 = 2.8$ nm comprising cetylpyridiniumchloride (CpCl) and octanol (Oct) (CpCl/Oct = 0.95 w/w) are diluted in brine ([NaCl = 0.2 M]) and decorated with Synperonic F68 (Serva) ($(EO_{76}) - (PO)_{29} - (EO)_{76}$ where EO is ethylene oxide and PO is propylene oxide) as amphiphilic copolymer. The bilayer volume fraction $\phi$ and the copolymer/surfactant weight ratio $\alpha$ range from 9 to 23% and 0 to 1.6 respectively. So the lamellar structure is preserved over large ranges of polymer and surfactant concentrations. Interestingly, a gel-like behaviour is located in the ($\alpha$, $\phi$) phase diagram over a

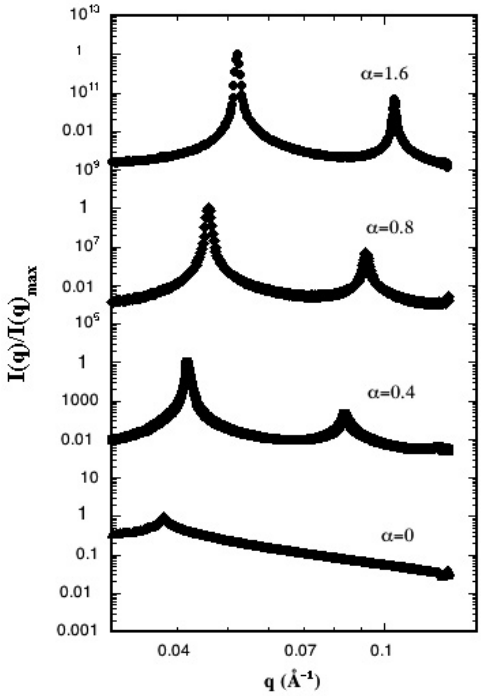


**Figure 2.** SAXS patterns of a series of lamellar samples of constant (surfactant + alcohol) weight ratio 16% for four different values of polymer to (surfactant + alcohol) weight ratio $\alpha$ (salinity $= 0.2$ mol l$^{-1}$); $m_{\mathrm{oct}}/m_{\mathrm{CPCl}} = 0.95$ g/g.

range of threshold copolymer/surfactant weight ratios that depends on the membrane fraction. The marked variation of the mechanical properties of the bulk lamellar phase is accompanied by modifications of the optical structure. Ramos *et al* [13] have demonstrated that the gel consists of polydisperse space-filling packing of lamellar onions. So the effects of the polymer layers on the physical properties of the lamellar phase are two-fold. On the one hand they modify the elastic properties of the individual membranes: (i) they soften the bilayer's mean curvature bending modulus (formation of onions) and (ii) they stretch and therefore thin down the membranes. On the other hand, the presence of polymer layers grafted on the membranes strongly enhances the repulsive Helfrich interaction between the fluid membranes by increasing the effective bilayer thickness. The effect is strong even at very low polymer concentration.

Figure 2 shows a series of SAXS patterns of lamellar samples at constant weight fraction of surfactants $w_{\mathrm{s}} = 16\%$ along a line of increasing polymer to amphiphile weight ratio $\alpha$. Two interesting features are observed. First the Bragg peaks of the lamellar phase progressively shift to higher $q$ values as $\alpha$ increases: this result can be quantitatively explained by the bilayer's thinning due to the competition between stretching of the polymer brush along the smectic direction and stretching of the membrane in the lateral direction; this effect provides a new simple method to estimate the area stretching modulus of fluid membrane and has been reported in detail in [11]. Second, the addition of copolymer correlates with the sharpening of the first Bragg peak and the emergence of higher harmonics in the scattering profile; it is observed whatever the dilution of the lamellar phase. So, this phenomenon deals with the polymer-induced interaction between bilayers.

In high salt brine (a few $10^{-1}$ mol $l^{-1}$) the electrostatic interaction is screened beyond distances much shorter than the smectic periodicity so the stability of the lamellar phase arises from the Helfrich interactions between membranes:

$$V_{\mathrm{Helf}} = C_{\mathrm{H}} \frac{(kT)^2}{\kappa (d-\delta)^2} \tag{6}$$

where $d$ is the smectic period, $\delta$ is the bilayer thickness, and $\kappa$ is the mean bending modulus of a single bilayer. The value of the numerical coefficient $C_{\mathrm{H}}$ calculated by Helfrich is $C_{\mathrm{H}} = 3\pi^2/128 \approx 0.231$ [14]. More recently, Monte Carlo simulations [15, 16] and field theoretical calculations [17, 18] give a smaller value $C_{\mathrm{H}} \approx 0.106$. In a lamellar phase each bilayer is confined between its two neighbours of the smectic stack; this phenomenon restricts the amplitude of the thermal bending fluctuations of the membrane and is the origin of the Helfrich interaction. This allows us to define the collision length which represents the average distance between two adjacent collision of a membrane between its neighbours [19]:

$$\lambda_{\mathrm{c}} = \sqrt{\frac{(2\pi)^3 \kappa}{2kT}} \bar{d} = \alpha_{\mathrm{c}} \bar{d} \tag{7}$$

where $\bar{d} = d - \delta$ is the average distance between the opposite surfaces of two adjacent bilayers.

Quantitative treatments of neutron scattering patterns allow one to measure the dimensionless Caillé parameter [20] $\eta$ defined in terms of the smectic elastic constants [21, 22]. Interestingly, when the Helfrich interaction is the dominant interlamellar interaction, $\eta$ follows the simple purely geometrical expression [23]:

$$\eta = \frac{4}{3}\left(1 - \frac{\delta}{d}\right)^2. \tag{8}$$

Notice that in equation (8), the prefactor $\frac{4}{3}$ corresponds to the Helfrich value $C_{\mathrm{H}} = 3\pi^2/128$.

In order to study the polymer-mediated repulsive interaction quantitatively we have fitted the SANS patterns of various series of samples (in heavy water) of constant weight fractions of membrane ($5\% < w_{\mathrm{s}} < 25\%$) along lines of increasing polymer to amphiphile weight ratio $\alpha$ (data shown in [12]) using either [21] or [22] for the more dilute samples. Doing so we obtained the variation of $\eta$ as a function of $\alpha$ for various membrane concentrations. In all series of samples the Caillé parameter decreases sharply as $\alpha$ increases until it reaches a plateau for $\alpha \approx \alpha^* \approx 0.5$ (crossover between the mushroom and brush regime). The measurements of $\eta$ are in agreement with the picture where the two grafted polymer layers on both sides of each bilayer modify the Helfrich interaction by a simple renormalization of the bare membrane thickness. This means that in equation (8) the bare membrane thickness $\delta_0$ should be simply replaced by an effective membrane thickness $\delta_{\mathrm{eff}}$:

$$\delta_{\mathrm{eff}} = \delta_0 + 2h \tag{9}$$

where $h$ is the *effective* thickness of the polymer layer attached on each side of a membrane. In figure 3, we have plotted the variation of this effective polymer thickness $h$ obtained from the measurements of $\eta$:$h = [d(1 - \sqrt{(3/4)\eta}) - \delta_0]/2$.

At low $\alpha$, that is in the very dilute mushroom regime ($\sigma \ll \sigma^*$), $h$ increases very rapidly as the polymer surface density increases, until it levels off into a plateau at the mushroom/brush transition, that is, as soon as the mushrooms begin to overlap and form a continuous layer on both sides of the membrane. We notice that the plateau value $h \approx 21$ Å roughly equals the radius of gyration of the PEO tails ($R_{\mathrm{G}} \approx 19$ Å). This saturation effect in the brush regime is related to the lateral stretching of the membrane which opposes the perpendicular stretching of polymer tails in the brush regime (for more details see [11]). More interesting is the mushroom regime. Experimentally for $w_{\mathrm{s}} = 20\%$, $h = 28.3(\sigma/\sigma^*)^{0.4}$ Å in the mushroom regime. In

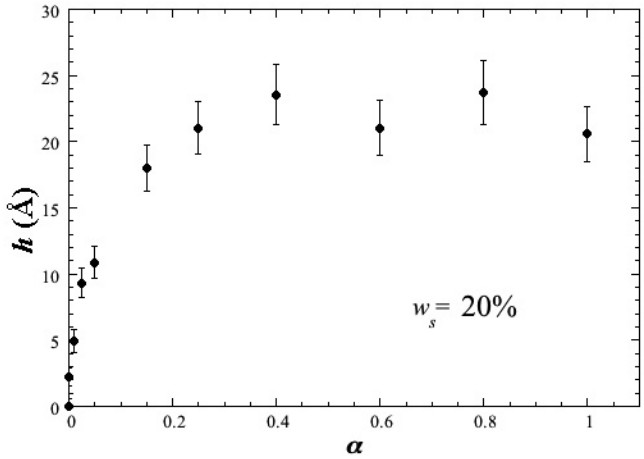


**Figure 3.** Plot of the effective thickness $h$ of the polymer layer versus the polymer/membrane weight ratio $\alpha$ obtained from equations (8) and (9) and the measurements of $\eta$ for a series of samples of constant membrane weight fraction $w_s = 20\%$.

this dilute regime, the polymer layer decorating the membrane is strongly inhomogeneous. Nevertheless, as shown in figure 3, the strong enhancement of the effective thickness at very low polymer grafting density seems to indicate that each mushroom (which can be viewed as a hemispherical patch of radius $R_G$) induces a local thickening of the decorated membrane of the order of $R_G$ *on an area much larger than the natural area of the patch* $\pi R_G^2$. This effect arises from the *finite* bending rigidity of the membrane which induces in-plane $(x, y)$ correlation in the position $z$ of one given bilayer. Indeed, each mushroom adsorbed on a *confined* membrane restricts the amplitude of its thermal fluctuations; the amplitude of this restriction is of the order of the size of the mushroom, $l \simeq R_G$. From equation (7), this restriction concerns a piece of the membrane centred on the mushroom of area $\pi \lambda_{mush}^2 = \pi(\alpha_c \bar{d})^2$, where $\alpha_c \gg 1$. This means that because of the finite bending rigidity of the membrane and the low compressibility of the polymer coils, a given mushroom affects collision between two neighbouring membranes not only at its own position, but on a 'ghost' pancake centred on the position of the mushroom with a radius of the order of the collision length $\lambda_{mush}$ defined by the thickness of the mushroom.

Unfortunately, a statistical theory of stacks of non-homogeneous compressible membranes is lacking. However, a simple heuristic model can be made to capture the essential physical ingredients of this effect. We can model the decorated membrane in the mushroom regime as a uniformly bumped membrane. A bump with axial symmetry is centred on each mushroom with a Gaussian shape of height $R_G$ and width at half-height $\lambda = \frac{4}{3}\lambda_{mush}$, and with a disc of area $\Sigma = \pi D^2/4$ being the base of a bump. $D$ is the average distance between grafted chains. So the effective thickness of the bumped membrane is:

$$h = \overline{h} = \frac{1}{\Sigma}\int_0^D 2\pi R_G \exp\left(-\frac{r^2}{\lambda^2}\right) dr = \frac{9}{8}\alpha_c^2 R_G \varphi_{pol}\left[1 - \exp\left(-\frac{8}{9\alpha_c^2\varphi_{pol}}\right)\right] \tag{10}$$

where $\overline{h}$ is the mean thickness of the bumped membrane and $\varphi_{pol} = \sigma/\sigma^*$.

In figure 4 we have plotted (full curve) the theoretical variation of $\eta$ with respect to $\alpha$ in the mushroom regime, given by the set of equations (8)–(10), together with the experimental points (symbols) for four different membrane concentrations. For all series we used the same value $\alpha_c = 3$ as the single fitting parameter. Despite its simplicity, the model of a bumped membrane describes well the strong decrease of the Caillé parameter in the regime of very dilute

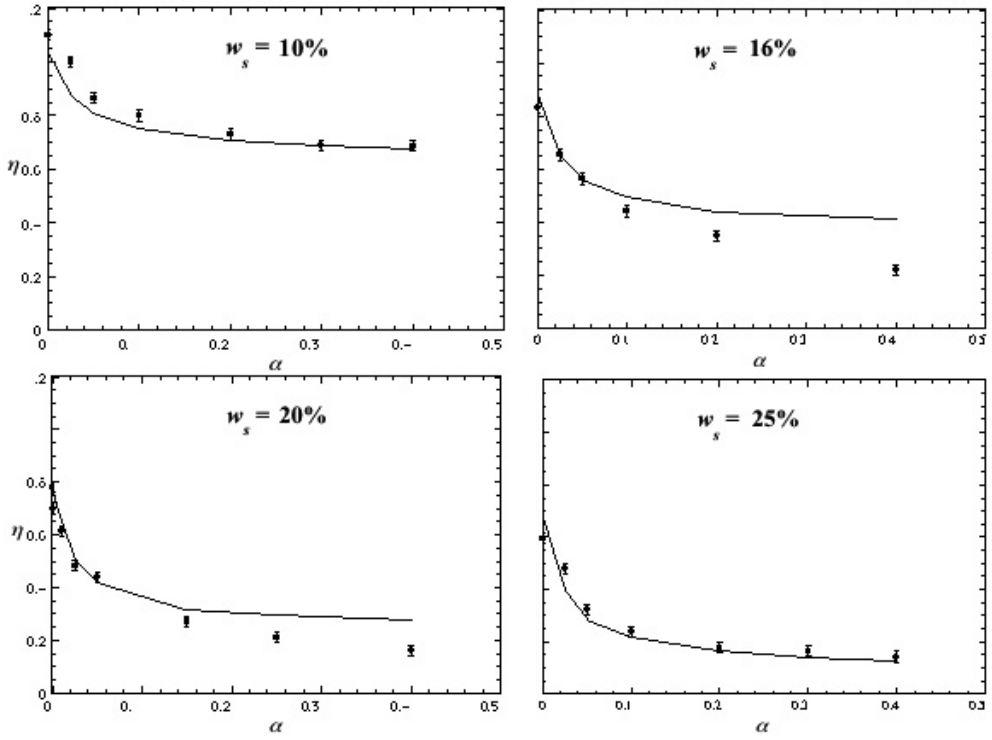


**Figure 4.** Variation of the Caillé parameter $\eta$ in the mushroom regime (symbols) and model (full curves) given by equations (8)–(10). For all series, the same fitting parameter is used: $\alpha_c = 3$.

mushrooms ($\alpha \ll 0.4$) and in the all studied dilution range ($10\% < w_s < 25\%$). Interestingly, a similar strong effect has also been observed when the membranes are decorated with rigid peptides [24].

## 4. Hairy wormlike micelles

The detailed reports of this section can be found in [25–27]. Hairy wormlike micelles consist of long flexible surfactant cylinders (wormlike micelles) decorated with amphiphilic copolymers. Solutions of wormlike micelles exhibit strong analogies with solutions of conventional polymers both for their structural and rheological properties [28]. Because surfactant self-assemblies scatter light and neutrons much more strongly than polymers, surfactant wormlike micelles have appeared as a convenient model system for the study of the structure of polymer solutions. Recently, we have shown that hairy wormlike micelles are also a model polymer solution for addressing the role of polydispersity in the scaling of the law for the elastic plateau modulus of entangled polymer solutions [29]. In this section I will focus on the steric repulsion between cylinders which is evidenced by the emergence of a broad peak in the structure factor of a semi-dilute solution of hairy wormlike micelles.

We use a mixture of CpCl as surfactant and sodium salicylate (NaSal) diluted in brine [NaCl] = 0.5 mol $l^{-1}$, at fixed molar ratio [NaSal]/[CpCl] = 0.5. This system is known to form long and flexible micelles even at low concentration [30]. We add to this host phase various amounts of triblock amphiphilic copolymer, Synperonic F108 (produced by Serva), which consists of two identical polyoxyethylene (PEO) blocks of 127 monomers each symmetrically

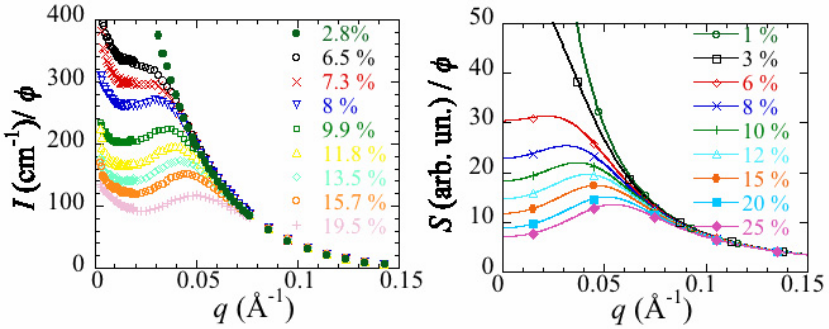


**Figure 5.** (a) Experimental scattering profiles and (b) theoretical structure factors, normalized by surfactant volume fraction $\phi$. In (a), $\alpha = 1\%$; in (b), the amplitude and range of the Gaussian potential are $U_0 = 800kT$ and $\delta = 34$ Å, respectively.

bonded to a central hydrophobic block of polyoxypropylene (PPO) of 48 monomers. The radius of gyration of a PEO block is $R_G \approx 26$ Å. By means of SANS we have shown that the local cylindrical structure of the micelles is maintained upon copolymer addition, with a constant radius of their hydrophobic core ($r_C \approx 21$ Å). We define $\phi$, the volume fraction of surfactant, and $\alpha$, the molar ratio of PEO blocks to surfactant molecules. In our experiments $\phi$ and $\alpha$ have ranges 0.22–40% and 0–4.2%, respectively. All experiments presented here were done in the semi-dilute regime ($\phi$ larger than the overlap concentration $\phi^*$). The crossover between the mushroom and brush structure is estimated to be at $\alpha^* \approx 1.5\%$, and both regimes are therefore probed in our experiments. The temperature is fixed at $T = 30\,^{\circ}$C. SANS experiments have been performed on the spectrometer PACE at the Laboratoire Léon Brillouin (Saclay France) and on the D11 beam line at the Institut Laue-Langevin (Grenoble France). The contrast in the scattered intensity is between the hydrophobic core and the solvent (the copolymer layer covering the micelles is not directly probed).

Again, there is a large domain in the $(\alpha, \phi)$ phase diagram where the samples remain isotropic, transparent, and monophasic [25]. In this monophasic domain, we have measured the scattering profile for samples with constant copolymer density but with various surfactant volume fractions $\phi$ as shown in figure 5(a) for $\alpha = 1\%$. The scattering profile is monotonically decreasing at low $\phi$, and above a threshold surfactant volume fraction $\phi_c$ a correlation peak is observed at finite wavevector. The intensity of the peak increases with $\phi$ and its position $q^*$ is moved to higher wavevector when $\phi$ increases. Figure 6(a) shows the variation of the scattering profile at a fixed surfactant volume fraction $\phi = 9\%$ when the copolymer intensity is increased. A peak emerges above a threshold copolymer molar ratio and becomes more and more pronounced and narrow as $\alpha$ increases. Moreover, the peak position varies only weakly with the copolymer to surfactant ratio.

Because of the high ionic strength (0.5 M), electrostatic interactions are screened and are thus not relevant in our experiments. The correlation peak observed experimentally originates therefore from the copolymer layer adsorbed onto the micelles. This layer creates a soft steric short range repulsion between the micelles, with a range of the order of the polymer layer thickness. To analyse more quantitatively the scattering profiles we use the random phase approximation theory (RPA) to compute the structure factor of polymeric chains (here the wormlike micelles) interacting via a short range repulsion.

RPA theory is a powerful tool for obtaining the statistical properties of concentrated solutions of polymers in a mean field approximation [31]. We apply this theory to semi-

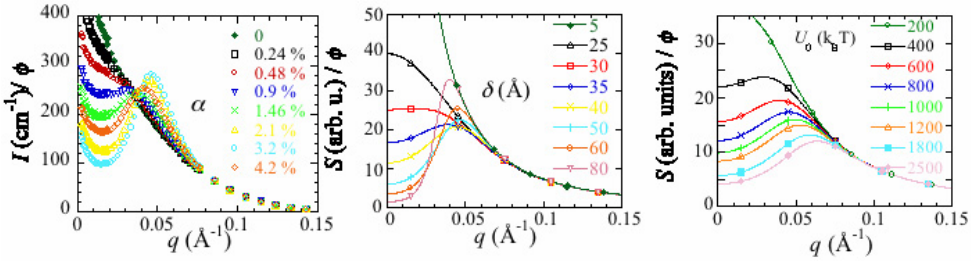


**Figure 6.** (a) Experimental scattering profiles and (b), (c) theoretical structure factors, normalized by surfactant volume fraction $\phi$. In (a), $\alpha = 1\%$ and curves are labelled by copolymer (F108) over surfactant ratio $\alpha$. In (b) and (c) $\phi = 10\%$. In (b) the amplitude of the potential is $U_0 = 800kT$, and curves are labelled by the range of the potential $\delta$. In (c) the range of the potential is $\delta = 34$Å and the curves are labelled by the amplitude of the potential $U_0$.

dilute solutions of hairy wormlike micelles. For a wormlike micelle, the statistical unit (or 'monomer') to consider is a portion of surfactant cylinder of length $l_K$ equal to twice the persistence length ($l_K \approx 380$ Å). We write the mean-field interaction potential $U(r)$ between two 'monomers' separated by $r$ as the sum of a classical excluded-volume term potential for polymers in good solvent and a soft short range potential to account for the specific contribution of the copolymer layer: $U(r) = v_0\delta(r) + U_0 \exp(-r^2/2\delta^2)$, where $v_0$ is the excluded-volume parameter. The range $\delta$ of the Gaussian potential should be of the order of the steric layer thickness. We moreover expect both $\delta$ and $U_0$ to increase as the amount of copolymer $\alpha$ increases. We note that a Gaussian form for the potential has been recently justified for some soft interacting objects, such as polymer coils [32], flexible dendrimers [33] or star polymers [34]. A Gaussian shape also has the advantage of leading to a simple analytical expression for the structure factor $S(q)$:

$$VS^{-1}(q) = VS_0^{-1}(q) + v_0 + U_0(2\pi\delta)^{3/2} \exp\left(-\frac{(q\delta)^2}{2}\right) \tag{11}$$

where $S_0(q) = NV\rho_0 f\left[(qR_G)^2\right]$ is the structure factor of ideal chains; $f(x) = \frac{2}{x^2}(e^{-x}+x-1)$ is the Debye function, $V$ the volume of the solution, $N$ the mean number of 'monomers' per micelle, $\rho_0$ the mean density of 'monomers' and $R_G$ the ideal radius of gyration of the micelles (the last three parameters can easily be expressed as functions of $\phi$ and $l_K$). The structure factor displays a peak for surfactant volume fraction larger than a threshold value $\phi_c = (\pi r_0^2 l_K^3)/(6(2\pi)^{3/2}\delta^5 U_0)$, and the position $q^*$ of the peak is given by

$$q^* = \frac{\sqrt{2}}{\delta}\sqrt{\ln\left(\frac{\phi}{\phi_c}\right)}. \tag{12}$$

A comparison with experimental data shows that the model captures the essential experimental features. These are, on the one hand, the $\alpha$-dependent threshold concentration above which a peak appears and the $\phi$-dependence of the shape and the peak position $q^*$ (figure 5(b)). On the other hand, increasing $\delta$ (respectively $U_0$) at fixed amplitude $U_0$ (respectively fixed range $\delta$) leads to the emergence of a peak in the structure factor and to an increase of its intensity as shown in figure 6(b) (respectively figure 6(c)). In the two cases, similarly to what is obtained experimentally upon increasing $\alpha$, the parameters $\delta$ and $U_0$ have poor influence on the peak position. A even more quantitative analysis of the data can be performed if we assume that the experimental peak position in the scattered intensity is correctly described by the theoretical structure factor. For surfactant volume fraction above $\phi_c$, we use equation (12)

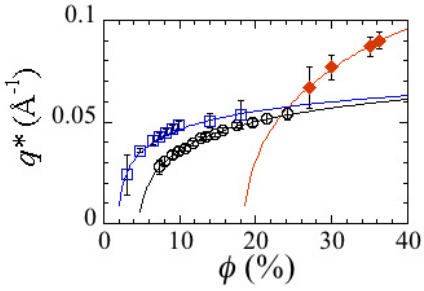


**Figure 7.** Variation of the peak position with surfactant volume fraction for samples without copolymers (diamonds), with $\alpha = 1\%$ (empty circles), and with $\alpha = 3.2\%$ (empty squares). The symbols are experimental points and the curves are best fits using equation (12).

to fit the experimental $\phi$-dependence of $q^*$ with $\delta$ and $U_0$ as fitting parameters. As shown in figure 7, a very good fit is obtained for the experimental data obtained for hairy micelles decorated with different amounts of copolymer as well as for naked micelles (in the case of the naked micelles, a correlation peak is observed only at very large concentration $\phi > 24\%$, and the fittings parameters correspond to a high and narrow potential in agreement with the fact that, in this case, the steric interaction originates from the dense thin shell of surfactant polar heads). A detailed discussion on the values of the fitting parameters both for decorated and naked cylinders can be found in [27]. Finally, one evaluates the thickness $h$ of the polymer layer as the distance at which the Gaussian potential equals $1kT$ (thus $h$ depends solely on $U_0$ and $\delta$). One finds that $h$ increases with $\alpha$ and has a correct order of magnitude.

## 5. Conclusion

The motivation of this paper was to show some new features induced by grafted polymer layers on the physical properties of surfactant self-assemblies with simple morphologies. Decorated polymer layers strongly modify both the elastic properties of the surfactant films and the interactions between the mesoscopic surfactant aggregates. I have emphasized several points:

- Hairy self-assemblies are in *thermal* equilibrium. Therefore, the relevant contributions of the polymer layer to the bending parameters of the surfactant membrane are those calculated at constant chemical potential of the decorated copolymer. Consequently, at low polymer coverage, the effective bending modulus does not change upon the addition of copolymer, whereas the spontaneous curvature significantly increases.
- Grafted copolymer layers induce steric interaction between surfactant self-assemblies as expected. However, this steric interaction has some peculiarities with respect to the more classical steric interaction in colloidal dispersions. In hairy lamellar phases, this interaction is *long range*, because of the fluctuating character of the fluid membranes. Moreover, the steric interaction is strong even at very low polymer coverage due to the finite bending rigidity of the membrane.
- Hairy surfactant self-assemblies may provide experimental models to get a better understanding of some aspects of colloidal science. For instance, we have shown that hairy wormlike micelles are good candidates for studying the structure of polymer solutions interacting via a soft repulsive potential. The approach we used to understand the structure factor of polymer-decorated cylindrical micelles could be used in a variety of 'hairy linear objects', such as cylindrical copolymer micelles or comblike polymers.

## Acknowledgments

The work described in this paper was realized with many collaborators: Jacqueline Appell, Francisco Castro-Roman, Gladys Massiera, Estelle Pitard, Grégoire Porte and Laurence Ramos. I thank all of them. Local contacts L Auvray and D Lairez on line PACE at Laboratoire Léon Brillouin-CEA-CNRS, and B Demé, R May and J Zipfel on line D11 at Insitut Laue Langevin are acknowledged for their help during the SANS experiments.

## References

[1] Appell J, Ligoure C and Porte G 2004 *J. Stat. Mech.: Theor. Exp.* P08002
[2] Milner S T and Safran S A 1987 *Phys. Rev.* A **36** 4371
[3] Safran S A 1983 *J. Chem. Phys.* **78** 2073
[4] Gradzielski M, Langevin D and Farago B 1996 *Phys. Rev.* E **53** 3900
[5] Lipowsky R 1995 *Europhys. Lett.* **30** 197
[6] Hiergeist C and Lipowsky R 1996 *J. Physique* II **6** 1465
[7] Porte G and Ligoure C 1995 *J. Chem. Phys.* **102** 4290
[8] Auth T and Gomper G 2003 *Phys. Rev.* E **68** 051801
[9] Joannic R, Auvray L and Lasic D 1997 *Phys. Rev. Lett.* **78** 3402
[10] Castro-Roman F, Porte G and Ligoure C 1999 *Phys. Rev. Lett.* **82** 109
[11] Castro-Roman F and Ligoure C 2001 *Europhys. Lett.* **53** 483
[12] Castro-Roman F, Porte G and Ligoure C 2001 *Langmuir* **17** 5045
[13] Ramos L, Roux D, Olmsted P D and Cates M E 2004 *Europhys. Lett.* **66** 888
[14] Helfrich W 1978 *Z. Naturf.* a **33** 305
[15] Gomper G and Kroll D M 1989 *Europhys. Lett.* **9** 59
[16] Janke W, Kleinert H and Meinhard M 1989 *Phys. Lett.* B **217** 525
[17] Kleinert H 1999 *Phys. Lett.* A **257** 269
[18] Bachman M, Leinert H and Pelster A 1999 *Phys. Lett.* A **261** 127
[19] Granek R 1997 *J. Physique* II **7** 1761
[20] Caillé A 1972 *C. R. Acad. Sci. Paris* B **274** 1733
[21] Nallet F, Laversanne R and Roux D 1993 *J. Physique* II **3** 487
[22] Castro-Roman F, Porcar L, Porte G and Ligoure C 2004 *Eur. Phys. J.* E submitted
[23] Roux D and Safinya C R 1988 *J. Physique* **49** 307
[24] Tsapis N, Urbach W and Ober R 2001 *Phys. Rev.* E **63** 041903
[25] Massiera G, Ramos L and Ligoure C 2002 *Langmuir* **18** 5687
[26] Massiera G, Ramos L, Pitard E and Ligoure C 2003 *J. Phys.: Condens. Matter* **15** S225
[27] Massiera G, Ramos L, Ligoure C and Pitard E 2003 *Phys. Rev.* E **68** 021803
[28] Cates M E and Candau S J 1990 *J. Phys.: Condens. Matter* **2** 6869 and references therein
[29] Massiera G, Ramos L and Ligoure C 2002 *Europhys. Lett.* **57** 127
[30] Rehage H and Hoffman H 1988 *J. Phys. C: Solid State Phys.* **92** 4712
[31] Edwards S F 1966 *Proc. Phys. Soc.* **88** 265
[32] Bolhuis P G, Hansen J-P and Meijer J 2001 *J. Chem. Phys.* **114** 4296
[33] Likos C N, Rosenfeldt S, Dingeouts N, Ballauff M, Lindner P, Werner N and Vogtle F 2002 *J. Chem. Phys.* **117** 1869
[34] Graf H and Löween H 1998 *Phys. Rev.* E **57** 5744